Accepted by PASP

Analysis of the Cramér-Rao lower uncertainty bound in the joint estimation of astrometry and photometry

Rene A. Mendez[1]

Departamento de Astronomía, Facultad de Ciencias Físicas y Matemáticas, Universidad de Chile, Casilla 36-D, Santiago, Chile

rmendez@u.uchile.cl

Jorge F. Silva

Department of Electrical Engineering, Av. Tupper 2007, Santiago, Chile
Information and Decision System Group
Universidad de Chile

josilva@ing.uchile.cl

Rodrigo Orostica

Departamento de Astronomía, Facultad de Ciencias Físicas y Matemáticas, Universidad de Chile, Casilla 36-D, Santiago, Chile

rorostica@ing.uchile.cl

and

Rodrigo Lobos

Department of Electrical Engineering, Av. Tupper 2007, Santiago, Chile
Information and Decision System Group
Universidad de Chile

rlobos@ing.uchile.cl

ABSTRACT

In this paper we use the Cramér-Rao lower uncertainty bound to estimate the maximum precision that could be achieved on the joint simultaneous (or 2D) estimation of photometry and astrometry of a point source measured by a linear CCD detector array.

[1]On leave at the European Southern Observatory, Casilla 19001, Santiago, Chile.

We develop exact expressions for the Fisher matrix elements required to compute the Cramér-Rao bound in the case of a source with a Gaussian light profile. From these expressions we predict the behavior of the Cramér-Rao astrometric and photometric precision as a function of the signal and the noise of the observations, and compare them to actual observations - finding a good correspondence between them.

From the Cramér-Rao bound we obtain the well known fact that the uncertainty in flux on a Poisson-driven detector, such as a CCD, goes approximately as the square root of the flux. However, more generally, higher order correction factors that depend on the ratio B/F or F/B (where B is the background flux per pixel and F is the total flux of the source), as well as on the properties of the detector (pixel size) and the source (width of the light profile), are required for a proper calculation of the minimum expected uncertainty bound in flux. Overall the Cramér-Rao bound predicts that the uncertainty in magnitude goes as $(S/N)^{-1}$ under a broad range of circumstances.

As for the astrometry we show that its Cramér-Rao bound also goes as $(S/N)^{-1}$ but, additionally, we find that this bound is quite sensitive to the value of the background - suppressing the background can greatly enhance the astrometric accuracy.

We present a systematic analysis of the elements of the Fisher matrix in the case when the detector adequately samples the source (oversampling regime), leading to closed-form analytical expressions for the Cramér-Rao bound. We show that, in this regime, the joint parametric determination of photometry and astrometry for the source become decoupled from each other, and furthermore, it is possible to write down expressions (approximate to first order in the small quantities F/B or B/F) for the expected minimum uncertainty in flux and position. These expressions are shown to be quite resilient to the oversampling condition, and become thus very valuable benchmark tools to estimate the approximate behavior of the maximum photometric and astrometric precision attainable under pre-specified observing conditions and detector properties.

Subject headings: Joint Photometry and Astrometry, Cramér-Rao bound, Data Analysis and Techniques, Astronomical Techniques, Stars

1. Introduction

In this paper we extend the 1D Cramér-Rao analysis done in Mendez et al. (2013) to the 2D case of simultaneous photometry and astrometry estimation on a linear CCD detector. The goal is to provide an estimation setting that is more realistic than that presented in Mendez et al. (2013), while still being tractable analytically so that useful closed-form expressions can be derived and interpreted from the analysis. This scenario allows us also to explore, in a simple manner, the extent of the inter-dependence between astrometry and photometry, from the point of view of the Cramér-Rao error bound under different instrumental and detection regimes.

In general, the Cramér-Rao lower variance bound can be used to cover a broad span of applications, ranging from instrument design for specific target accuracy goals, to observational planning, and to data analysis benchmarking (see., e.g., Perryman et al. (1989), Jakobsen et al. (1992), Zaccheo et al. (1995), Adorf (1996)). For example, the Cramér-Rao bound can be used to predict how a particular design choice (pixel size, readout noise, etc.) influences the photometric and astrometric performance of the planned instrument, it permits the prediction of lower bounds to photometric errors for point sources (and for surface photometry of extended objects), and places lower bounds to the precision with which the position of point sources can be measured (depending on their shape), be it as isolated objects, or in a cluster. The Cramér-Rao formalism also allows us to determine the influence of sub-pixel dither patterns on the astrometric and photometric errors (Mendez et al. (2013) and this paper, Section 3.1). Finally, the Cramér-Rao lower bound can be used to test the statistical adequacy of different data reduction and analysis algorithms, or even the reliability of our data: Those pipelines that can not attain the Cramér-Rao bound may not be statistically optimum.

One of the limitations of the Cramér-Rao formalism is that, in general, by itself, it does not offer a way to construct an estimator that reaches the bound (unless the parametric setting satisfies a necessary and sufficient condition, see Stuart, et al. (2004, p.12)). However, what one can do is to try various estimators, in a more or less heuristic way, and compare its empirical performance, in terms of its variance, with that predicted by the Cramér-Rao bound, to determine how close it approaches the bound. An important point to note here is that a biased estimator may have a variance lower than that predicted by the Cramér-Rao bound (for a nice and simple example of this see Stoica and Moses (1990)). Therefore, a very tight estimator should be viewed with caution, since it may be indicative that our *estimations* are actually biased, rendering parameter estimations that suffer from a systematic effect.

Our paper is organized as follows: Section 2 introduces the basic setting of problem, its notations and basic terminology and results. In addition this section focuses on the simple 1D case of photometric estimation, and revisits key results of the 1D astrometric problem. Section 3 is the main section and elaborates and analyzes the expression of the Cramér-Rao bound for the joint astrometry and photometry estimation problem. Finally in Section 4 we summarize our main conclusions.

2. Preliminaries

In this Section we introduce our notation and provide the basic setting that will be used in the joint astrometric and photometric estimation problem in Section 3.

2.1. Parameter estimation and the multivariate Cramér-Rao bound

Let I_i (with $i = 1, ..., n$) be a collection of independent observations (or measurements) that follow a parametric probability mass function $f_{\vec{\theta}}$ defined on $\mathbb{N}$. The parameters to be estimated from the measurements $\vec{I} = \{I_i : i = 1, ..., n\}$ will be denoted by $\vec{\theta} = (\theta_1, \theta_2, ..., \theta_m) \in \mathbb{R}^m$. Then given the measurements, let us consider $\hat{\vec{\theta}}(I_1, ..., I_n) = (\hat{\theta}_1, \hat{\theta}_2, ..., \hat{\theta}_m)$ to be an unbiased estimator of the parameters $\vec{\theta}$. If $L(\vec{I}; \vec{\theta})$ is the likelihood of the observations $\vec{I}$ given the parameters $\vec{\theta}$, and we can verify that $L(\vec{I}; \vec{\theta})$ satisfies the condition:

$$\mathbb{E}_{\vec{I} \sim f^n_{\vec{\theta}}} \left(\frac{\partial \ln L(\vec{I}; \vec{\theta})}{\partial \theta_i} \right) = 0 \quad \forall \, \theta_i \;\; (i = 1...m) \tag{1}$$

then, the celebrated Cramér-Rao bound states that (Rao 1945; Cramér 1946):

$$Var(\hat{\theta}_i(\vec{I})) \geq \sigma^2_{\theta_i} \equiv [\mathcal{I}_{\vec{\theta}}(n)^{-1}]_{i,i} \tag{2}$$

where $\mathcal{I}_{\vec{\theta}}(n)$ denotes the *Fisher information* matrix of the data about the vector of parameters $\vec{\theta}$, given by:

$$[\mathcal{I}_{\vec{\theta}}(n)]_{i,j} = \mathbb{E} \left(\frac{\partial \ln L(\vec{I}; \vec{\theta})}{\partial \theta_i} \cdot \frac{\partial \ln L(\vec{I}; \vec{\theta})}{\partial \theta_j} \right) \;\; (i, j = 1...m). \tag{3}$$

2.2. Joint photometric and astrometric estimation setting

Given a point source parameterized by its position x_c and flux $\tilde{F}$, the central estimation problem here is to jointly estimate the pair $(x_c, \tilde{F})$ using the measurements of a photon integrating device with n pixels (such as a CCD). This device measures the vector $\{I_i : i = 1, ..., n\}$ corresponding to fluxes (counts) per pixel. In this digital setting, we model $\{I_i : i = 1, ..., n\}$ as independent and not identically distributed random variables, where I_i follow a Poisson distribution with expected value given by the function $\lambda_i(x_c, \tilde{F})$. More precisely, the likelihood function of this estimation problem is given by:

$$L(\vec{I}; (x_c, \tilde{F})) = f_{\lambda_1(x_c, \tilde{F})}(I_1) \cdot f_{\lambda_2(x_c, \tilde{F})}(I_2) \cdots f_{\lambda_n(x_c, \tilde{F})}(I_n) \tag{4}$$

where $f_\lambda(I) = \frac{e^{-\lambda} \cdot \lambda^I}{I!}$ is the Poisson probability mass function. Note that equation (4) models the fact that the measurements are independent but in general not identically distributed.

If $\tilde{F}_i(x_c, \tilde{F})$ represents the expected flux from the source (at pixel i, in photo-e$^-$) and $\tilde{B}_i$ is the total integrated background (at pixel i, in e$^-$), the expected flux at pixel i follows an additive noise model given by:

$$\lambda_i(x_c, \tilde{F}) = \tilde{F}_i(x_c, \tilde{F}) + \tilde{B}_i, \tag{5}$$

Note that in equation (5), $\tilde{B}_i$ includes the contribution from the detector (read-out noise and

dark current) and the the sky background[1], and consequently it is independent of $(x_c, \tilde{F})$. On the other hand, $\tilde{F}_i(x_c, \tilde{F}) = \tilde{F} \cdot g_i(x_c)$ where $g_i(x_c)$ is characterized by the one dimensional normalized "Point Spread Function" (PSF hereafter), denoted by $\phi(x)$ arcsec^{-1}, through:

$$g_i(x_c) = \int_{x_i - \frac{\Delta x}{2}}^{x_i + \frac{\Delta x}{2}} \Phi(x - x_c)\, dx. \tag{6}$$

In equation (6), x_i denotes the central coordinate of pixel $i \in \{1, ..., n\}$, Δx is the pixel size and $\int_{-\infty}^{+\infty} \Phi(x)\, dx = 1$. In this work we will assume a Gaussian PSF, i.e.,

$$\Phi(x) = \frac{1}{\sqrt{2\pi}\,\sigma}\, e^{-\frac{1}{2}\left(\frac{x}{\sigma}\right)^2} \quad [\text{arcsec}^{-1}] \tag{7}$$

which is a reasonable assumption in the context of ground-based data (Mendez et al. 2010). Then, from (6), we have the following identity that will be used in the computation of the Cramér-Rao bound in (3): $\forall i \in \{1, ..., n\}$

$$\frac{dg_i}{dx_c}(x_c) = \frac{1}{\sqrt{2\pi}\,\sigma} \left(e^{-\gamma(x_i^- - x_c)} - e^{-\gamma(x_i^+ - x_c)} \right) \quad [\text{arcsec}^{-1}] \tag{8}$$

where $\gamma(x) \equiv \frac{1}{2}(\frac{x}{\sigma})^2$, with $x_i^- = x_i - \frac{\Delta x}{2}$ and $x_i^+ = x_i + \frac{\Delta x}{2}$.

Finally, we identify $\tilde{F}$ as the total flux of the source:

$$\sum_{i=1}^{n} \tilde{F}_i(x_c, \tilde{F}) = \tilde{F} \sum_{i=1}^{n} g_i(x_c) = \tilde{F} \sum_{i=1}^{n} \int_{x_i - \frac{\Delta x}{2}}^{x_i + \frac{\Delta x}{2}} \Phi(x)\, dx \approx \tilde{F} \int_{-\infty}^{+\infty} \Phi(x)\; dx = \tilde{F}. \tag{9}$$

where we have assumed that the detector properly samples the PSF.

2.3. Photometric estimation

In this section we elaborate on the simplified case of estimating the flux of a source, $\tilde{F}$ (in units of photo-e$^-$), assuming that x_c is known with very high accuracy. Hence the (expected) source flux on pixel i can be written in the form:

$$\tilde{F}_i(\tilde{F}) = \tilde{F} \cdot g_i(x_c) \quad (i = 1...n) \tag{10}$$

where the positional parameter x_c is a known quantity in this context. Then we can verify equation (1) and derive the Cramér-Rao lower bound for the estimation of $\tilde{F}$ as follows:

[1]See the concrete expression in Mendez et al. (2013, equation (23)).

Proposition 1 *Let $\hat{\tilde{F}}(\vec{I})$ be an arbitrary unbiased estimator of $\tilde{F}$, then:*

$$Var(\hat{\tilde{F}}(\vec{I})) \geq \sigma^2_{\tilde{F}_{1D}} \equiv \frac{1}{\sum_{i=1}^{n} \frac{g_i^2}{\tilde{F}\cdot g_i + \tilde{B}_i}} \tag{11}$$

$$= 2\pi\sigma^2 \cdot \tilde{B} \cdot \frac{1}{\sum_{i=1}^{n} \frac{J_i(x_c)^2}{\left(1 + \frac{1}{\sqrt{2\pi}\,\sigma} \cdot \frac{\tilde{F}}{\tilde{B}} \cdot J_i(x_c)\right)}}, \tag{12}$$

where for the last expression, the background $\tilde{B}$ is considered to be uniform across the array[2]*, i.e., $\tilde{B}_i = \tilde{B}$ for all i, and where $J_i(x_c)$ is given by:*

$$J_i(x_c) \equiv \int_{x_i^-}^{x_i^+} e^{-\gamma(x-x_c)}\, dx \;\; [arcsec] \tag{13}$$

(The proof is presented in Appendix A).

From equation (11) it is straightforward to compute the two extreme regimes, i.e., background or source-dominated, which are given, to first order in the small quantity $\tilde{F}/\tilde{B}$ or $\tilde{B}/\tilde{F}$ respectively, by:

$$\sigma^2_{\tilde{F}_{1D}} \simeq \begin{cases} \frac{\tilde{B}}{\sum_{i=1}^{n} g_i^2} \cdot \left(1 + \frac{\tilde{F}}{\tilde{B}} \cdot \frac{\sum_{i=1}^{n} g_i^3}{\sum_{i=1}^{n} g_i^2}\right) & \text{if } \tilde{F} \ll \tilde{B} \\ \tilde{F} \cdot \left(1 + n \cdot \frac{\tilde{B}}{\tilde{F}}\right) & \text{if } \tilde{F} \gg \tilde{B} \end{cases} \tag{14}$$

where have assumed a constant background as a function of position in the array, $\tilde{B}$, and used the fact that $\sum_{i=1}^{n} g_i = 1$[3]. Interestingly, the second relation above shows the well known fact that the uncertainty in flux goes approximately as the square root of the flux itself (measured in e^-), when the background is negligible.

2.4. Astrometric estimation

Here we summarize the main results derived in Mendez et al. (2013) for the problem of estimating the position of the source x_c when the total flux $\tilde{F}$ is known by the observer. In terms of notation,

---

[2]The analysis to correctly characterize the background for computing the Cramér-Rao bound in astronomical applications is elaborated in Mendez et al. (2013, Sec. 4).

[3]Note that, since $\tilde{B}$ is the background *per pixel*, the term $n \cdot \tilde{B}$ represents the total contribution of the background to the measured flux. In this context, n represents not the full pixel array but, rather, the portion of the array over which the flux of the source is being calculated (see definition of $N_{\rm pix}$ on equation (20) below). If this is the case, then $\sum_{i=1}^{n} g_i$ is not necessarily equal to one, but rather it corresponds to the fraction of the flux enclosed within the n pixels. Hopefully the "aperture" is chosen to include most of the flux $\tilde{F}$, or a suitable correction is applied (e.g., through a curve-of-growth) to compensate for the missing fraction of this flux.

we can consider the expected flux at pixel i by $\lambda_i(x_c) = \tilde{F}_i(x_c) + \tilde{B}_i$ where $\tilde{F}_i(x_c) = \tilde{F} \cdot g_i(x_c)$ and $\tilde{F}$ is known. Then we can state the following:

Proposition 2 *(Mendez et al. (2013, equations (10) and (21))) Let $\hat{x_c}(\vec{I})$ be an arbitrary unbiased estimator of x_c, then:*

$$Var(\hat{x}_c(\vec{I})) \geq \sigma^2_{x_{c_{1D}}} \equiv \frac{1}{\sum_{i=1}^{n} \frac{\left(\tilde{F}\,\frac{dg_i}{dx_c}(x_c)\right)^2}{\tilde{F}\,g_i(x_c) + \tilde{B}_i}} \tag{15}$$

$$= 2\pi\sigma^2 \cdot \frac{\tilde{B}}{\tilde{F}^2} \cdot \frac{1}{\sum_{i=1}^{n} \frac{\left(e^{-\gamma(x_i^- - x_c)} - e^{-\gamma(x_i^+ - x_c)}\right)^2}{\left(1 + \frac{1}{\sqrt{2\pi}\,\sigma}\frac{\tilde{F}}{\tilde{B}} \cdot J_i(x_c)\right)}}. \tag{16}$$

In the last expression we have assumed a uniform background $\tilde{B}$ across pixels, as in equation (12).

In the high resolution regime, i.e., $\Delta x/\sigma \ll 1$, the following limiting (weak and strong source) closed-form expression for $\sigma^2_{x_{c_{1D}}}$ can be derived (see details in Mendez et al. (2013, Sec. 4.1.)):

$$\sigma^2_{x_{c_{1D}}} \approx \begin{cases} \frac{\sqrt{\pi}}{2\,(2\,\ln 2)^{3/2}} \cdot \frac{\tilde{B}}{\tilde{F}^2} \cdot \frac{FWHM^3}{\Delta x} & \text{if } \tilde{F} \ll \tilde{B} \\ \frac{1}{8\,\ln 2} \cdot \frac{1}{\tilde{F}} \cdot FWHM^2 & \text{if } \tilde{F} \gg \tilde{B}, \end{cases} \tag{17}$$

where $FWHM = 2\sqrt{2\ln 2}\,\sigma$ denotes the "Full-Width at Half-Maximum" parameter, which is associated with the image quality at the observing site.

3. Joint astrometric and photometric Cramér-Rao bound

Let us now consider the more realistic case of having to jointly estimate the flux $\tilde{F}$ and astrometric position x_c on a linear detector. Note that the calculation of the inverse Fisher matrix in equation (2) implies computing its determinant, which, in general, involve all the elements of the matrix. This property highlights the potential cross-dependency in the errors of quantities that one may naively consider, in principle, as decoupled, like, e.g., 1D astrometry and photometry presented in Section 2. This will be further explored in Section 3.3.

From equation (4) we have that $\ln L(\vec{I}; (x_c, \tilde{F})) = \sum_{i=1}^{n} \Big(I_i \cdot \ln \lambda_i(x_c, \tilde{F}) - \lambda_i(x_c, \tilde{F}) - \ln I_i!\Big)$. In this case, it is straightforward to verify that the conditions in equation (1) are satisfied for both position and flux (see (Mendez et al. 2013, equation (8)) for x_c and equation (A2) for $\tilde{F}$). Then we can state the following result:

Proposition 3 *The Fisher matrix coefficients for the joint estimation of astrometry and photometry for a Gaussian PSF, can be written, in exact form, as follow:*

$$\begin{aligned}
\mathcal{I}_{1,1} &= \frac{1}{2\pi\sigma^2}\cdot\frac{GF^2}{B}\cdot\sum_{i=1}^{n}\frac{\left(e^{-\gamma(x_i^-x_c)}-e^{-\gamma(x_i^+-x_c)}\right)^2}{\left(1+\frac{1}{\sqrt{2\pi}\,\sigma}\cdot\frac{F}{B}\cdot J_i(x_c)\right)}\\
\mathcal{I}_{1,2}=\mathcal{I}_{2,1} &= \frac{1}{2\pi\sigma^2}\cdot\frac{F}{B}\cdot\sum_{i=1}^{n}\frac{\left(e^{-\gamma(x_i^-x_c)}-e^{-\gamma(x_i^+-x_c)}\right)\cdot J_i(x_c)}{\left(1+\frac{1}{\sqrt{2\pi}\,\sigma}\cdot\frac{F}{B}\cdot J_i(x_c)\right)}\\
\mathcal{I}_{2,2} &= \frac{1}{2\pi\sigma^2}\cdot\frac{1}{GB}\cdot\sum_{i=1}^{n}\frac{J_i(x_c)^2}{\left(1+\frac{1}{\sqrt{2\pi}\,\sigma}\cdot\frac{F}{B}\cdot J_i(x_c)\right)}
\end{aligned}\tag{18}$$

(The derivation is presented in Appendix B).

In the expressions in equation (18), we have introduced the (inverse-)gain of the detector G in units of e^-/ADUs (Analog to Digital Units, or 'counts" on the detector), such that B and F (no tilde) are in ADUs and are defined by $\tilde{F} = G \cdot F$ and $\tilde{B} = G \cdot B$ respectively. The Cramér-Rao limit in flux, computed from the above expressions will still be in units of e^-.

Note that in the 1D astrometric case, the only meaningful term is $\mathcal{I}_{1,1}$, which is exactly the inverse of the Cramér-Rao variance derived in Proposition 2, equation (16). Likewise, in the 1D photometric case, the only meaningful term is $\mathcal{I}_{2,2}$, which is exactly the inverse of the Cramér-Rao variance as shown by equation (12) in Proposition 1 above.

3.1. Analysis and interpretation of the 2D Cramér-Rao bound

In Mendez et al. (2013), it was shown that astrometry is optimal (in the sense that the positional error budget is minimal), when the object image is sitting near the edge of a pixel, since positional information is residing in the slopes of the object image profile. Interestingly, using the above expressions, we find an effect for photometry which is just the opposite of that in astrometry: The lowest variance is found when the source is located towards the center of a pixel, rather than towards its boundary, this is shown in Figure 1. The effect is however quite subtle, and tends to be worse for severely undersampled images. This could be a relevant aspect for studies requiring extremely high-accuracy (relative) photometry (e.g., for observations of exo-planet occultations), and specially when observing with somewhat undersampled imagers (see Section 3.3).

At this point it is timely to introduce the definition of signal-to-noise ratio, S/N, as a relevant parameter to interpret the Cramér-Rao bound. It is possible to show that the S/N for a Gaussian

source is given by[4]:

$$\frac{S}{N}(u_+) = \frac{P(u_+)\cdot F}{\sqrt{\frac{P(u_+)\cdot F}{G} + \frac{u_+}{\sqrt{\ln 2}\,G}\frac{FWHM}{\Delta x}\left(f_s\Delta x + \frac{RON^2}{G}\right)}}, \tag{19}$$

where RON is the read-out noise per pixel of the detector, in units of e^-, f_s is the sky background (in units of ADUs/arcsec), and u_+ is a dimensionless quantity related to the number of pixels of the region under which the signal of the source is being measured, $N_{\rm pix}$, given by (see Mendez et al. (2013, equation (27))):

$$u_+ = \frac{1}{\sqrt{\ln 2}\,N_{\rm pix}}\cdot\frac{FWHM}{\Delta x}, \tag{20}$$

and where $P(u_+)$ represents the fraction of the total flux F sampled in the $N_{\rm pix}$, given by $P(u) = \frac{2}{\sqrt{\pi}}\int_0^u e^{-v^2}\,dv$.

The overall trend of the 2D Cramér-Rao limit on astrometry and photometry for one particular choice of parameters is depicted as a function of the S/N of the source (measured at 90% of its flux) in Figure 2. As shown in Mendez et al. (2013, equation (45)), the astrometric uncertainty will be either $\propto B^{1/2}/F$ at small flux (and small S/N), or $\propto F^{-1/2}$ at high flux (and large S/N). Therefore, considering the definition of S/N, we will have that $\sigma_{x_c} \propto (S/N)^{-1}$. However, as also shown in the 1D-astrometric setting in Mendez et al. (2013, equation (21)), the astrometric Cramér-Rao depends not only on the S/N but also on the value of the background itself. This is clearly seen on Figure 2, were we compute the Cramér-Rao bound for two values of f_s: We find that, for this choice of parameters, the astrometric gain by completely suppressing the sky-background (of course an ideal situation representing the most extreme case one could think of, yet useful to define strict lower bounds) is significant, almost 20% in σ_{x_c} for both values of the $FWHM$, at a $S/N \sim 50$. The figure also shows that as the S/N increases the solid and dashed lines converge, implying that, as the relative importance of the sky-background becomes smaller, the potential gain in astrometric accuracy through minimizing the background is reduced, as intuitively expected.

Rather than looking at the Cramér-Rao limit in flux directly, it is customary to express this quantity in terms of the uncertainty in magnitudes, computed as:

$$\sigma_{\hat{m}} \equiv \frac{2.5}{2}\cdot\left(\log\left(\tilde{F}+\sigma_{\tilde{F}}\right) - \log\left(\tilde{F}-\sigma_{\tilde{F}}\right)\right), \tag{21}$$

which is quite close to, but in our opinion more robust, than the classical $\frac{1}{0.4\ln 10}\cdot\frac{\sigma_{\tilde{F}}}{\tilde{F}}$, since the uncertainties are not necessarily very small for this last expression to be true. The results for $\sigma_{\hat{m}}$ are almost indistinguishable from each other in terms of $FWHM$ or f_s, for the choice of parameters in Figure 2. This result is however expected: Equation (14) shows that the uncertainty in flux will

[4]See Mendez et al. (2013, Section 4)) for details.

be either dominated by the square root of the background at small flux (and small S/N), or by the square root of the total flux at high flux (and large S/N). Therefore, since $\sigma_{\hat{m}} \propto \frac{\sigma_{\tilde{F}}}{\tilde{F}}$, we will have that $\sigma_{\hat{m}} \propto (S/N)^{-1}$, mostly independent of the background (unlike the case of astrometry, see previous paragraph) or other parameters. We also note that, after a rapid decline in error as the S/N increases, the asymptotic behavior of $\sigma_{\hat{m}}$ for very large S/N may explain, in part, why it is so difficult to achieve photometric precisions smaller than a few milli-mag. While at $S/N \sim 100$ we predict $\sigma_{\hat{m}} \sim 11$ [mmag], at $S/N \sim 200$ we would have $\sigma_{\hat{m}} \sim 5$ [mmag], consistent with actual measurements, as quoted by Zhilyaev et al. (2005) (see also Warner (2006, Section 4 and Table 4.1)).

While the expressions for the inverse of the Fisher matrix can be readily calculated from equation (18), they do not offer much insight into the approximate dependency of the Cramér-Rao bound on relevant quantities, like the $FWHM$ or the S/N of the source, or the detector pixel size Δx. For this purpose, it is useful to resort to the small pixel (high resolution) approximation of a Gaussian PSF, which is done in the next Section.

3.2. The 2D Cramér-Rao bound in the small pixel (high resolution) approximation

If we assume that the pixel array oversamples the source, i.e., if $\Delta x/\sigma \ll 1$, then one has that:

$$g_i(x_c) \simeq \Phi(x_i - x_c) \cdot \Delta x \tag{22}$$

$$\frac{\partial g_i(x_c)}{\partial x_c} \simeq \frac{(x_i - x_c)}{\sigma^2} \cdot g_i(x_c). \tag{23}$$

As it can be easily verified, under this approximation the elements of the Fisher matrix become:

$$\begin{aligned}
\mathcal{I}_{1,1} &= \frac{\tilde{F}^2}{\sigma^4} \cdot \sum_{i=1}^{n} \frac{(x_i - x_c)^2}{(\tilde{F} g_i(x_c) + \tilde{B}_i)} \cdot g_i(x_c)^2 \\
\mathcal{I}_{1,2} &= \frac{\tilde{F}}{\sigma^2} \cdot \sum_{i=1}^{n} \frac{(x_i - x_c)}{(\tilde{F} g_i(x_c) + \tilde{B}_i)} \cdot g_i(x_c)^2 \\
\mathcal{I}_{2,2} &= \sum_{i=1}^{n} \frac{1}{(\tilde{F} g_i(x_c) + \tilde{B}_i)} \cdot g_i(x_c)^2.
\end{aligned} \tag{24}$$

We note that the term $\mathcal{I}_{1,2}$ in equation (24), being a function of an odd power of $(x_i - x_c)$, is expected to be very small if the source is well sampled by the detector, an important fact that will be fully exploited in the following analysis (see also Section 3.3). On the other hand, the dependence on $\tilde{F} g_i(x_c) + \tilde{B}_i$ in the denominator of equation (24) makes it difficult to get simple analytical expressions for them. However, things simplify notably in the two extreme regimes of flux- and background-dominated sources, which we will examine in turn in the next sub-sections.

3.2.1. Flux dominated sources in the Small Pixel (High Resolution) approximation

In this case, a first-order series development of the term $(\tilde{F} g_i(x_c) + \tilde{B}_i)^{-1}$ in equation (24), in terms of the quantity $\tilde{B}/\tilde{F}$ (assumed to be $\ll 1$), yields the following:

$$\begin{aligned}
\mathcal{I}_{1,1} &= \frac{\tilde{F}}{\sigma^4} \cdot \left(\sum_{i=1}^{n} (x_i - x_c)^2 \cdot g_i(x_c) - \frac{\tilde{B}}{\tilde{F}} \cdot \sum_{i=1}^{n} (x_i - x_c)^2 \right) \\
\mathcal{I}_{1,2} &= \frac{1}{\sigma^2} \cdot \left(\sum_{i=1}^{n} (x_i - x_c) \cdot g_i(x_c) - \frac{\tilde{B}}{\tilde{F}} \cdot \sum_{i=1}^{n} (x_i - x_c) \right) \\
\mathcal{I}_{2,2} &= \frac{1}{\tilde{F}} \cdot \left(1 - n \cdot \frac{\tilde{B}}{\tilde{F}} \right). \qquad (25)
\end{aligned}$$

This series development allows us to write some of the terms in the above expressions in an analytical closed-form, which greatly facilitates the evaluation of the Cramér-Rao bound. For our Gaussian PSF we will have, in the high resolution approximation, that:

$$\begin{aligned}
\sum_{i=1}^{n} (x_i - x_c) \cdot g_i(x_c) &\approx \frac{1}{\sqrt{2\pi}\sigma} \cdot \lim_{\Delta x \to 0} \sum_{i=1}^{n} (x_i - x_c) \cdot e^{-\frac{(x_i - x_c)^2}{2\,\sigma^2}} \cdot \Delta x \\
&= \frac{1}{\sqrt{2\pi}\sigma} \cdot \int_{-\infty}^{+\infty} (x - x_c) \cdot e^{-\frac{(x - x_c)^2}{2\,\sigma^2}}\, dx \\
&= 0, \qquad (26)
\end{aligned}$$

while, on the other hand:

$$\begin{aligned}
\sum_{i=1}^{n} (x_i - x_c)^2 \cdot g_i(x_c) &\approx \frac{1}{\sqrt{2\pi}\sigma} \cdot \lim_{\Delta x \to 0} \sum_{i=1}^{n} (x_i - x_c)^2 \cdot e^{-\frac{(x_i - x_c)^2}{2\,\sigma^2}} \cdot \Delta x \\
&= \frac{1}{\sqrt{2\pi}\sigma} \cdot \int_{-\infty}^{+\infty} (x - x_c)^2 \cdot e^{-\frac{(x - x_c)^2}{2\,\sigma^2}}\, dx \\
&= \sigma^2. \qquad (27)
\end{aligned}$$

Replacing (26) and (27) into equation (25), we end up with:

$$\begin{aligned}
\mathcal{I}_{1,1} &= \frac{\tilde{F}}{\sigma^4} \cdot \left(\sigma^2 - \frac{\tilde{B}}{\tilde{F}} \cdot \sum_{i=1}^{n} (x_i - x_c)^2 \right) \\
\mathcal{I}_{1,2} &= -\frac{1}{\sigma^2} \cdot \frac{\tilde{B}}{\tilde{F}} \cdot \sum_{i=1}^{n} (x_i - x_c) \\
\mathcal{I}_{2,2} &= \frac{1}{\tilde{F}} \cdot \left(1 - n \cdot \frac{\tilde{B}}{\tilde{F}} \right). \qquad (28)
\end{aligned}$$

With these coefficients, it is easy to see that the determinant, required for the evaluation of the inverse of the Fisher matrix, can be written, to first order in $\tilde{B}/\tilde{F}$, as follows:

$$\mathcal{I}_{11} \cdot \mathcal{I}_{22} - \mathcal{I}_{12}^2 \approx \frac{1}{\sigma^4} \cdot \left(\sigma^2 - \frac{\tilde{B}}{\tilde{F}} \cdot \sum_{i=1}^{n} (x_i - x_c)^2 \right) \cdot \left(1 - n \cdot \frac{\tilde{B}}{\tilde{F}} \right), \tag{29}$$

then, it can be verified that the Cramér-Rao bound for astrometry becomes:

$$\sigma_{x_c}^2 = [\mathcal{I}_{(x_c,\tilde{F})}(n)^{-1}]_{1,1} \approx \frac{1}{8\ln 2} \cdot \frac{1}{GF} \cdot \left(1 + \frac{1}{8\ln 2} \cdot \frac{B}{F} \cdot \frac{\sum_{i=1}^{n} (x_i - x_c)^2}{FWHM^2} \right) \cdot FWHM^2. \tag{30}$$

We note that equation (30) is equivalent to equation (17-bottom line) for the 1D case, but where the extra term in parenthesis in equation (30) accounts for the fact that in the present case we have retained the terms up to first order in the small quantity (i.e., if $B/F \to 0$, both equations coincide exactly). The validity of equation (30) in comparison with both prior theoretical estimates as well as real astrometry, has already been discussed in Mendez et al. (2013). Here we would like to add that the results by Gatewood et al. (1985), based on measurements with the Multichannel Astrometric Photometer, fully support our prediction that the astrometric accuracy improves as the inverse of the square root of the photon counts, as predicted by equation (30).

Completely analogously, the Cramér-Rao bound for photometry, provided that $n \cdot B \ll F$ (meaning that the flux is being estimated within a reasonable aperture, containing most of the flux, but avoiding to incorporate background far away from the main core of the source), becomes:

$$\sigma_{\tilde{F}}^2 = [\mathcal{I}_{(x_c,\tilde{F})}(n)^{-1}]_{2,2} \approx GF \cdot \left(1 + n \cdot \frac{B}{F} \right). \tag{31}$$

This equation is equivalent to the 1D expression shown in equation (14-bottom line), and it shows that, in the small pixel approximation, the determination of the flux is completely decoupled from the astrometry (see Section 3.3 for a further discussion of this), leading to the well-known fact that the expected standard deviation of the flux goes as the square root of the flux itself (measured in e^-) when the source dominates the counts, a feature which is characteristic of a Poisson-driven detection process.

3.2.2. Background dominated sources in the Small Pixel (High Resolution) approximation

Let us know explore the other regime, i.e., when $\tilde{F}/\tilde{B} \ll 1$. Following the same steps as in the previous section, it is simple to verify that equation (24) become:

$$\begin{aligned}
\mathcal{I}_{1,1} &= \frac{\tilde{F}^2}{\tilde{B}\sigma^4} \cdot \left(\sum_{i=1}^{n} (x_i - x_c)^2 \cdot g_i(x_c)^2 - \frac{\tilde{F}}{\tilde{B}} \cdot \sum_{i=1}^{n} (x_i - x_c)^2 \cdot g_i(x_c)^3 \right) \\
\mathcal{I}_{1,2} &= \frac{\tilde{F}}{\tilde{B}\sigma^2} \cdot \left(\sum_{i=1}^{n} (x_i - x_c) \cdot g_i(x_c)^2 - \frac{\tilde{F}}{\tilde{B}} \cdot \sum_{i=1}^{n} (x_i - x_c) \cdot g_i(x_c)^3 \right)
\end{aligned}$$

$$\mathcal{I}_{2,2} = \frac{1}{\tilde{B}} \cdot \left(\sum_{i=1}^{n} g_i(x_c)^2 - \frac{\tilde{F}}{\tilde{B}} \cdot \sum_{i=1}^{n} g_i(x_c)^3 \right). \quad (32)$$

It can be readily seen from equation (26) that a summation involving any power of $g_i(x_c)$, modulated by an odd function of $(x_i - x_c)$ will be zero in the high resolution regime, and therefore the off-diagonal term $\mathcal{I}_{1,2}$ in equation (32) will be zero in this case. The other summations in equation (32) can be easily calculated following the same procedure outlined in (26) and (27), for example:

$$\begin{aligned} \sum_{i=1}^{n} g_i(x_c)^2 &\approx \frac{\Delta x}{2\pi\sigma^2} \cdot \lim_{\Delta x \to 0} \sum_{i=1}^{n} e^{-\frac{(x_i - x_c)^2}{\sigma^2}} \cdot \Delta x \\ &= \frac{\Delta x}{2\pi\sigma^2} \cdot \int_{-\infty}^{+\infty} e^{-\frac{(x - x_c)^2}{\sigma^2}} \, dx \\ &= \frac{1}{2\sqrt{\pi}} \cdot \frac{\Delta x}{\sigma}, \end{aligned} \quad (33)$$

and, also:

$$\begin{aligned} \sum_{i=1}^{n} (x_i - x_c)^2 \cdot g_i(x_c)^2 &\approx \frac{\Delta x}{2\pi\sigma^2} \cdot \lim_{\Delta x \to 0} \sum_{i=1}^{n} (x_i - x_c)^2 \cdot e^{-\frac{(x_i - x_c)^2}{\sigma^2}} \cdot \Delta x \\ &= \frac{\Delta x}{2\pi\sigma^2} \cdot \int_{-\infty}^{+\infty} (x - x_c)^2 \cdot e^{-\frac{(x - x_c)^2}{\sigma^2}} \, dx \\ &= \frac{1}{4\sqrt{\pi}} \cdot \Delta x \cdot \sigma. \end{aligned} \quad (34)$$

The other terms in equation (32) can be calculated in an analogous way, obtaining:

$$\sum_{i=1}^{n} g_i(x_c)^3 \approx \frac{1}{2\sqrt{3}\pi} \cdot \left(\frac{\Delta x}{\sigma} \right)^2, \quad (35)$$

$$\sum_{i=1}^{n} (x_i - x_c)^2 \cdot g_i(x_c)^3 \approx \frac{\Delta x^2}{6\sqrt{3}\pi}. \quad (36)$$

Using the above values for the coefficients, the Cramér-Rao bound for astrometry is given by:

$$\sigma_{x_c}^2 = [\mathcal{I}_{(x_c, \tilde{F})}(n)^{-1}]_{1,1} \approx \frac{1}{4\ln 2} \sqrt{\frac{\pi}{2\ln 2}} \cdot \frac{B}{GF^2} \cdot \left(1 + \frac{4}{3} \sqrt{\frac{2\ln 2}{3\pi}} \cdot \frac{F}{B} \cdot \frac{\Delta x}{FWHM} \right) \cdot \frac{FWHM^3}{\Delta x}. \quad (37)$$

As it was mentioned in Section 3.2.1, here too, this equation reduces to the 1D equation in (17-top line), when the ratio $F/B \to 0$. On the other hand, the corresponding Cramér-Rao bound for photometry would be, in this case:

$$\sigma_{\tilde{F}}^2 = [\mathcal{I}_{(x_c, \tilde{F})}(n)^{-1}]_{2,2} \approx \sqrt{\frac{\pi}{2\ln 2}} \cdot GB \cdot \left(1 + 2 \sqrt{\frac{2\ln 2}{3\pi}} \cdot \frac{F}{B} \cdot \frac{\Delta x}{FWHM} \right) \cdot \frac{FWHM}{\Delta x}. \quad (38)$$

In equation (38), the ratio $(FWHM/\sqrt{\ln 2}\,\Delta x)$ represents the sampling of the PSF of the object[5] and we can see, from equation (20) that $u_+ = \sqrt{\pi/2} \approx 1.253$, which represents an aperture containing $\sim 92\%$ of the equivalent "flux" (given by $P(u_+)$). So, in this setting, too (as it was the case of equation (31)), the uncertainty in the flux goes as square root of the flux, which is however in this case mostly provided by the background. We also note that the term $B/\Delta x$ is approximately equal to the sky background in units of ADU/arcsec, therefore equation (38) implies a total aperture (diameter) that samples $\sqrt{\frac{\pi}{2\ln 2}} \approx 1.5$ times the $FWHM$ of the source.

3.3. Range of use of the high resolution Cramér-Rao bound

Given the simplicity of the equations derived in the previous sub-sections, it is important to define how quickly equations (30) and (31), or (37) and (38) deteriorate as we move away from their respective regimes of application. Interestingly enough, the approximate flux Cramér-Rao bound is a lot more insensitive to the assumptions involved than its astrometric counterpart. For example, a very weak source ($S/N = 3$) with a $FWHM = 1.0$ arcsec has a predicted Cramér-Rao bound uncertainty in flux of $\sim$27%, the same value as derived from equation (38), independently of Δx from 0.1 to 1.0 arcsec. In the same regime, the astrometric Cramér-Rao bound increases from $\sigma_{x_c} = 164$ mas to 321 mas for Δx from 0.1 to 1.0 arcsec, whereas equation (37) predicts $\sigma_{x_c} = 160$ mas (1 mas = 1 milli-arcsec). For strong sources ($S/N = 200$) the "exact" photometric Cramér-Rao bound (derived from equation (18)) predicts 0.5% uncertainty in flux, same as that given by equation (31), whereas the exact astrometric Cramér-Rao calculation shows an increase from 2.2 to 3.1 mas when Δx increases from 0.1 to 1.0 arcsec, while that predicted by equation (30) gives 1.9 mas. As a rule of thumb we find that, as long as $\Delta x/FWHM < 0.5$, equations (30) and (31), or (37) and (38) are quite reliable, and can be very useful as quick estimators.

Another aspect of the above discussion is that, as can be seen from the analysis presented in the previous two sub-Sections, a critical assumption of the adopted approximations in the high-resolution regime is the fact that, to first order on either $\tilde{B}/\tilde{F}$ or $\tilde{F}/\tilde{B}$, the coefficient $\mathcal{I}_{1,2} \sim 0$. Since the off-diagonal terms in the Fisher matrix represent the strength of the co-dependency among the parameters to be estimated (in this case position and flux), in practice this means that, under this assumption, the Cramér-Rao bound in astrometry and photometry become de-coupled from each other, thus converging to their respective 1D approximations. It is therefore interesting to explore approximately under which regime of parameters this assumption actually holds. For this purpose, in Figure 3 we show the behavior of the difference between the exact 2D expressions derived in Section 3, denoted by σ_{x_c} and $\sigma_{\tilde{F}}$, and their exact 1D, counterparts (equations (12) and (16)),

[5]More details in Mendez et al. (2013, equation (27)).

denoted by $\sigma_{x_{c_{1D}}}$ and $\sigma_{\tilde{F}_{1D}}$, computed for astrometry and photometry respectively as:

$$\begin{aligned}\Delta\sigma_x \equiv \frac{\sigma_{x_c} - \sigma_{x_{c_{1D}}}}{\sigma_{x_c}} &= \frac{\sqrt{\frac{\mathcal{I}_{2,2}}{\mathcal{I}_{1,1}\cdot\mathcal{I}_{2,2}-\mathcal{I}_{1,2}^2}} - \sqrt{\frac{1}{\mathcal{I}_{1,1}}}}{\sigma_{x_c}},\\ \Delta\sigma_{\tilde{F}} \equiv \frac{\sigma_{\tilde{F}} - \sigma_{\tilde{F}_{1D}}}{\sigma_{\tilde{F}}} &= \frac{\sqrt{\frac{\mathcal{I}_{1,1}}{\mathcal{I}_{1,1}\cdot\mathcal{I}_{2,2}-\mathcal{I}_{1,2}^2}} - \sqrt{\frac{1}{\mathcal{I}_{2,2}}}}{\sigma_{\tilde{F}}}.\end{aligned} \tag{39}$$

Note that, defined this way, both are dimensionless fractional quantities, and should be always ≥ 0.

It turns out that, numerically, the fractional values for $\Delta\sigma_x$ and $\Delta\sigma_{\tilde{F}}$ are quite similar as a function of Δx. As an example, in Figure 3, we see that the effect of neglecting the cross-term $\mathcal{I}_{1,2}$ for this particular setting, having a relatively high S/N, is only noticeable for under-sampled images but, as can be seen from the figure, in any case the difference is smaller than $\sim$15% under a wide-variety of reasonable conditions (see below for further details on this). We also notice that, as expected, the differences $\Delta\sigma_x$ and $\Delta\sigma_{\tilde{F}}$ depend (in a complex way) on the pixel offset, illustrating the effect of symmetry breaking in odd terms involving $(x_i - x_c)$ (recall Section 3.2.2). We have verified that, at lower S/N (~ 6), the effect is much steeper, and it occurs at smaller Δx, but it is still true that, for well sampled images ($\Delta x < FWHM$), the differences are minimal (less than 1%). The overall corollary of this exercise is that the 1D Cramér-Rao case for photometry and astrometry can be safely used for quick estimation purposes, instead of their more complex 2D cousin, being quite forgiving about the fine-pixel requirement $\Delta x/\sigma \ll 1$.

Since some recent large-area surveys and robotic telescopes are exploring the undersampled regime, e.g., SuperWASP[6], 13.7 arcsec/pix (described by Pollacco et al. (2006)), TRAPPIST[7], 0.64 arcsec/pix (described by Gillon et al. (2011)), the Catalina Real-Time Transient Survey[8], 0.98, 1.84 and 2.57 arcsec/pix (described by Djorgovski et al. (2011), or the La Silla-QUEST Variability Survey[9], 0.88 arcsec/pix (described by Baltay et al. (2013)) among others, it is interesting to quantify the impact of this design feature into the predicted Cramér-Rao bound. To estimate the effect of neglecting the cross-dependency between flux and astrometry, Table 1 compares the 1D and 2D Cramér-Rao limits as a function of the pixel size Δx, and the S/N of the source, adopting the same parameters as those of Figure 3. In the table, the astrometric Cramér-Rao is in units of mas, whereas the Cramér-Rao bound in flux is in %, defined by $100\cdot\frac{\sigma_{\tilde{F}}}{\tilde{F}}$ and $100\cdot\frac{\sigma_{\tilde{F}_{1D}}}{\tilde{F}_{1D}}$ respectively. Since, as discussed previously (see also Figure 3), the Cramér-Rao limit depends on the centering

[6]http://www.superwasp.org/

[7]http://www.orca.ulg.ac.be/TRAPPIST/

[8]http://crts.caltech.edu/

[9]http://hep.yale.edu/lasillaquest

of the source on the pixel, we have computed the Cramér-Rao limit for two representative pixel offsets, of 0.125 pix and 0.25 pix. As it can be seen from this table, at intermediate and high S/N the photometry is not appreciably affected by the pixel size, but we naturally see a gradual deterioration of the location accuracy as the pixel size increases. At low S/N the impact of pixel size (and pixel offsets) becomes critical for astrometry, and noticeable for photometry. Across the table we also see the impact of pixel offsets on the expected precision for both photometry and astrometry, in particular a "feature" already discussed in this and in our previous paper, namely that astrometry is better done near the pixel boundaries (large offsets), whereas photometry is better done near the pixel centers (small offsets). At a low $S/N = 5$ and very undersampled images ($\Delta x = 1.5$ arcsec), one may even argue that pixels offsets can make the difference between non-detection and detection of the source: Compare the formal astrometric Cramér-Rao value for a pixel offset of 0.125 pix, with $\sigma_{x_c} \sim 4$ arcsec, to the more reasonable value of $\sigma_{x_c} \sim 0.5$ arcsec for a pixel offset of 0.25 pix.

3.4. Effects of a variable PSF or a variable background

So far we have assumed that the PSF, mostly characterized in our scheme by its $FWHM$, is constant across the detector. However, in many cases, the telescope plus camera optical system may introduce variations in the $FWHM$ of the images at the focal plane (Schroeder 2013), and even changes on the shape of the PSF (e.g., aberrations). Also, focal reducers, commonly used in wide-field imagers, can introduce illumination problems that generate background variations on scales of the field-of-view of the detector (Selman 2004). Both of these effects will have an impact on the Cramér-Rao bound, depending on the position of the source relative to the optical axis of the camera, and it is therefore important to quantify them.

In the case of oversampled images, the effect on astrometry and photometry of changes in the $FWHM$ and the (local) background B can be readily calculated from equations (30) and (31), or (37) and (38). From these we see that, at high S/N, the astrometric Cramér-Rao bound scales approximately linearly with the $FWHM$ (while the photometry is independent of the $FWHM$), whereas at low S/N the impact on the expected astrometric precision due to changes on the width of the PSF gets amplified by a factor of 1.5. On the other hand, for well-exposed images, small background variations do not have an important impact on astrometry nor photometry, as intuitively expected, whereas for weak images we have that $\frac{\Delta\sigma_{x_c}}{\sigma_{x_c}} = \frac{\Delta\sigma_{\tilde{F}}}{\tilde{F}} = \frac{1}{2} \cdot \frac{\Delta B}{B}$.

For undersampled images, we have to resort to the exact expressions, given by equation (18). In Table (2) we show the effect of a change of 20% in the width of the PSF, or a 10% change in the background, on the predicted photometric and astrometric Cramér-Rao bounds, for an under-sampled image, with $FWHM = 0.5$ and $\Delta x = 1.0$ arcsec. We have computed this for the best-case scenario for photometry (source centered on a given pixel, upper part of the table), and for the best case scenario for astrometry (source centered on a pixel boundary, lower part of the table). As it can be seen from the table, the impact of these changes on the photometry (provided that the background is properly accounted for in the photometric measurements), is minimal. On

the other hand, for the best case astrometric setting, the 10% change in the $FWHM$ implies a $\sim$ 20% change in the astrometric Cramér-Rao limit, whereas this increases to as much as 50% for the worst case centering. Changes in background have a smaller, albeit non-negligible, impact on the astrometry, inducing a 5% increase in the Cramér-Rao limit regardless of the centering location. These results are at variance with the high-resolution behavior (see previous paragraph), which shows the importance of computing the Cramér-Rao bound in this specific situation for each particular case.

We finally note that, in all calculations above, we have still assumed a Gaussian PSF. A meaningful extension to other PSF shapes requires an extension of the Cramér-Rao calculation to a fully two-dimensional X-Y array, including the possibility of a cross-correlation term in the PSF between the X and Y coordinates (i.e., that the shape of the PSF is not necessarily oriented along any of the CCD axis, case of aberrated images), which we hope to explore in forthcoming papers.

4. Conclusions

We have developed general expressions for the Cramér-Rao minimum variance bound for the joint estimation of photometry and astrometry in a linear detector for a Gaussian source.

We show that the minimum expected photometric errors depend on the position of the source with respect to the pixel center, being larger if the source is located toward the pixel boundaries. The effect is subtle, and becomes more relevant for undersampled images. This result is exactly the opposite of what is found for the astrometric Cramér-Rao bound, and described thoroughly in Mendez et al. (2013, Section 3.3).

We demonstrate that both, astrometric and photometric (magnitudes) minimal error bounds, vary $\propto (S/N)^{-1}$, while the astrometry is, additionally, quite sensitive to the value of the background - suppressing the background can greatly enhance the astrometric accuracy.

When the detector adequately samples the source (oversampling regime), we show that the joint parametric determination of photometry and astrometry for the source become decoupled from each other, and furthermore, it is possible to write down closed-form expressions (approximate to first order in the small quantities F/B or B/F) for the expected minimum uncertainty estimation of the flux and position. We formally verify the known fact that the uncertainty in flux depends *mostly* on the square root of the flux, while for astrometry we recover the astrometry-only 1D Cramér-Rao results found by Mendez et al. (2013).

We show that the de-coupling of the Cramér-Rao bounds between σ_{x_c} and $\sigma_{\tilde{F}}$ is quite resilient to the assumption $\Delta x/FWHM \ll 1$ and, in fact, as long as we satisfy $\Delta x/FWHM < 0.5$, the cross term $\mathcal{I}_{1,2}$ in the Fisher information matrix is negligible. Given this result, we regard equations (30), (31), (37) and (38) as particularly useful benchmark estimators for the maximum attainable photometric and astrometric precision, given a detector setting and pre-specified obser-

vational conditions.

Finally, we explore the impact of variations in the spread of the PSF, or on the level of the background, upon the Cramér-Rao limit, and we derive expressions for the precision bound in some simple cases. We also show that, in general, astrometry is more sensitive (fractionally) than photometry due to variations in the $FWHM$ or the background.

A. Proof of Proposition 1: Cramér-Rao bound for flux

In order to insure that the conditions for the Cramér-Rao bound are met, we need to verify that the constraint in (1) is satisfied in regards to the parameter $\tilde{F}$ and, if so, we are allowed to use equations (2) and (3) to compute the Cramér-Rao bound. Using equation (4) and omitting the explicit dependency on x_c on all the variables there, we have for the parameter $\tilde{F}$ that:

$$\frac{d\ln L(\vec{I};\tilde{F})}{d\tilde{F}} = \frac{d}{d\tilde{F}}\left(\sum_{i=1}^{n}\left(I_i\cdot\ln\lambda_i(\tilde{F})-\lambda_i(\tilde{F})-\ln I_i!\right)\right) \tag{A1}$$

$$= \sum_{i=1}^{n} I_i\cdot\frac{1}{\lambda_i(\tilde{F})}\cdot\frac{d\lambda_i(\tilde{F})}{d\tilde{F}}-\sum_{i=1}^{n}\frac{d\lambda_i(\tilde{F})}{d\tilde{F}}. \tag{A2}$$

If $\mathbb{E}$ is the expected value with respect to the vector of observables $(I_1,...,I_n)$ given $\tilde{F}$, we indeed verify from the above expression that $\mathbb{E}_{I_1,...,I_n}\left(\frac{d\ln L(\vec{I};\tilde{F})}{d\tilde{F}}\right)=0$ because $\mathbb{E}(I_i)=\lambda_i(\tilde{F})$. Hence, we can apply equations (2) and (3).

First, we need to compute the Fisher information (3) of the data about $\tilde{F}$, which is given by:

$$\mathcal{I}_{\tilde{F}}(n)\equiv\mathbb{E}_{I_1,...,I_n\sim f^n_{\tilde{F}}}\left(\left(\frac{d\ln L(\vec{I};\tilde{F})}{d\tilde{F}}\right)^2\right) \tag{A3}$$

Noting that $d\lambda_i(\tilde{F})/d\tilde{F}=g_i$, from (A2) we will thus have:

$$\frac{d\ln L(\vec{I};\tilde{F})}{d\tilde{F}}=\sum_{i=1}^{n} g_i\cdot\frac{I_i}{\lambda_i}-1, \tag{A4}$$

where we have used the fact that $\sum_{i=1}^{n} g_i=1$ (see equation (9)). From this we can write:

$$\left(\frac{d\ln L(\vec{I};\tilde{F})}{d\tilde{F}}\right)^2 = \left(\sum_{i=1}^{n} g_i\cdot\frac{I_i}{\lambda_i}\right)^2-2\cdot\sum_{i=1}^{n} g_i\cdot\frac{I_i}{\lambda_i}+1$$

$$= \sum_{i=1}^{n}\sum_{j=1}^{n} g_ig_j\cdot\frac{I_iI_j}{\lambda_i\lambda_j}-2\cdot\sum_{i=1}^{n} g_i\cdot\frac{I_i}{\lambda_i}+1$$

$$= \sum_{i=1}^{n} g_i^2\cdot\frac{I_i^2}{\lambda_i^2}+\sum_{i=1}^{n}\sum_{j\neq i}^{n} g_ig_j\cdot\frac{I_iI_j}{\lambda_i\lambda_j}-2\cdot\sum_{i=1}^{n} g_i\cdot\frac{I_i}{\lambda_i}+1. \tag{A5}$$

Therefore,

$$\mathbb{E}\left(\frac{d\ln L(\vec{I};\tilde{F})}{d\tilde{F}}\right)^2 = \sum_{i=1}^{n} g_i^2+\sum_{i=1}^{n} g_i^2\cdot\frac{1}{\lambda_i}+\sum_{i=1}^{n}\sum_{j\neq i}^{n} g_ig_j-1$$

$$= \left(\sum_{i=1}^{n} g_i\right)^2+\sum_{i=1}^{n} g_i^2\cdot\frac{1}{\lambda_i}-1$$

$$= \sum_{i=1}^{n}\frac{g_i^2}{\lambda_i} \tag{A6}$$

where we have used the facts that $\mathbb{E}(I_i) = \lambda_i$, $\mathbb{E}(I_i^2) = \lambda_i^2 + \lambda_i$, and $\mathbb{E}(I_i \cdot I_j) = \mathbb{E}(I_i) \cdot \mathbb{E}(I_j) = \lambda_i \cdot \lambda_j$, this last expression since the pixel measurements are independent. With the above expression, and equation (A3), we see that:

$$\mathcal{I}_{\tilde{F}}(n) = \sum_{i=1}^{n} \frac{g_i^2}{\left(\tilde{F} \cdot g_i + \tilde{B}_i\right)}, \tag{A7}$$

from which the expression in equation (11), namely $\sigma^2_{\tilde{F}_{1D}} = \mathcal{I}_{\tilde{F}}(n)^{-1}$, follows directly.

B. Proof of Proposition 3: Fisher information matrix for joint astrometry and flux.

The likelihood function is given by $\ln L(\vec{I};(x_c,\tilde{F})) = \sum_{i=1}^{n}\Big(I_i\cdot\ln\lambda_i(x_c,\tilde{F}) - \lambda_i(x_c,\tilde{F}) - \ln I_i!\Big)$. The required partial derivatives are given by:

$$\frac{\partial \ln L(\vec{I};(x_c,\tilde{F}))}{\partial x_c} = \sum_{i=1}^{n}\left(\frac{I_i}{\lambda_i(x_c,\tilde{F})}\cdot\frac{\partial\lambda_i(x_c,\tilde{F})}{\partial x_c} - \frac{\partial\lambda_i(x_c,\tilde{F})}{\partial x_c}\right), \tag{B1}$$

and,

$$\frac{\partial \ln L(\vec{I};(x_c,\tilde{F}))}{\partial \tilde{F}} = \sum_{i=1}^{n}\left(\frac{I_i}{\lambda_i(x_c,\tilde{F})}\cdot g_i(x_c) - g_i(x_c)\right), \tag{B2}$$

where we have used the fact that since, by definition, $\lambda_i(x_c,\tilde{F}) = \tilde{F}\cdot g_i(x_c)+\tilde{B}_i$, then $\partial\lambda_i(x_c,\tilde{F})/\partial\tilde{F} = g_i(x_c)$.

We verify that, both $\mathbb{E}_{I_1,\ldots,I_n}\left(\frac{\partial \ln L(\vec{I};\tilde{F})}{\partial x_c}\right) = 0$ and $\mathbb{E}_{I_1,\ldots,I_n}\left(\frac{\partial \ln L(\vec{I};\tilde{F})}{\partial \tilde{F}}\right) = 0$ because $\mathbb{E}(I_i) = \lambda_i(\tilde{F})$. Hence, we can apply equations (2) and (3). To make mathematical notation easier, in what follows we identify the sub-index '1' with the parameter of spatial coordinate x_c, while the sub-index '2' refers to the parameter flux $\tilde{F}$. Consequently, the individual matrix terms are:

$$\begin{aligned}
\mathcal{I}_{1,1}(n) \equiv & \quad \mathbb{E}_{I_1,\ldots,I_n}\left(\left(\frac{\partial \ln L(\vec{I};x_c,\tilde{F})}{\partial x_c}\right)^2\right)\\
= & \quad \mathbb{E}_{I_1,\ldots,I_n}\left(\sum_i\sum_j\left(\frac{I_i\cdot I_j}{\lambda_i(x_c,\tilde{F})\cdot\lambda_j(x_c,\tilde{F})}\cdot\frac{\partial\lambda_i(x_c,\tilde{F})}{\partial x_c}\cdot\frac{\partial\lambda_j(x_c,\tilde{F})}{\partial x_c} - 2\cdot\frac{I_i}{\lambda_i(x_c,\tilde{F})}\cdot\frac{\partial\lambda_i(x_c,\tilde{F})}{\partial x_c}\cdot\frac{\partial\lambda_j(x_c,\tilde{F})}{\partial x_c}\right)\right)\\
& \quad + \sum_i\sum_j\frac{\partial\lambda_i(x_c,\tilde{F})}{\partial x_c}\cdot\frac{\partial\lambda_j(x_c,\tilde{F})}{\partial x_c}\\
= & \quad \mathbb{E}_{I_1,\ldots,I_n}\left(\sum_i\left(\frac{I_i}{\lambda_i(x_c,\tilde{F})}\cdot\frac{\partial\lambda_i(x_c,\tilde{F})}{\partial x_c}\right)^2\right) + \mathbb{E}_{I_1,\ldots,I_n}\left(\sum_i\sum_{j\neq i}\frac{I_i\cdot I_j}{\lambda_i(x_c,\tilde{F})\cdot\lambda_j(x_c,\tilde{F})}\cdot\frac{\partial\lambda_i(x_c,\tilde{F})}{\partial x_c}\cdot\frac{\partial\lambda_j(x_c,\tilde{F})}{\partial x_c}\right)\\
& \quad - \sum_i\sum_j\frac{\partial\lambda_i(x_c,\tilde{F})}{\partial x_c}\cdot\frac{\partial\lambda_j(x_c,\tilde{F})}{\partial x_c}\\
= & \quad \sum_i\frac{\left(\lambda_i(x_c,\tilde{F})+\lambda_i(x_c,\tilde{F})^2\right)}{\lambda_i(x_c,\tilde{F})^2}\cdot\left(\frac{\partial\lambda_i(x_c,\tilde{F})}{\partial x_c}\right)^2 + \sum_i\sum_{j\neq i}\frac{\partial\lambda_i(x_c,\tilde{F})}{\partial x_c}\cdot\frac{\partial\lambda_j(x_c,\tilde{F})}{\partial x_c} - \left(\sum_i\frac{\partial\lambda_i(x_c,\tilde{F})}{\partial x_c}\right)^2\\
= & \quad \sum_i\frac{1}{\lambda_i(x_c,\tilde{F})}\cdot\left(\frac{\partial\lambda_i(x_c,\tilde{F})}{\partial x_c}\right)^2
\end{aligned} \tag{B3}$$

where we have used, as in Appendix A, the facts that $\mathbb{E}(I_i) = \lambda_i$, $\mathbb{E}(I_i^2) = \lambda_i^2 + \lambda_i$, and $\mathbb{E}(I_i\cdot I_j) = \mathbb{E}(I_i)\cdot\mathbb{E}(I_j) = \lambda_i\cdot\lambda_j$, this last expression since the pixel measurements are un-correlated. In the case of a Gaussian PSF, it is easy to verify using equations (5), (6), (8), and (13) and replacing them in equation (B3) that:

$$\mathcal{I}_{1,1}(n) = \frac{1}{2\pi\sigma^2}\cdot\frac{GF^2}{B}\cdot\sum_{i=1}^{n}\frac{\left(e^{-\gamma(x_i^- - x_c)} - e^{-\gamma(x_i^+ - x_c)}\right)^2}{\left(1+\frac{1}{\sqrt{2\pi}\,\sigma}\cdot\frac{F}{B}\cdot J_i(x_c)\right)} \tag{B4}$$

For the cross term we have:

$$\mathcal{I}_{1,2}(n) \equiv \quad \mathbb{E}_{I_1,\ldots,I_n}\left(\frac{\partial \ln L(\vec{I};x_c,\tilde{F})}{\partial x_c}\cdot\frac{\partial \ln L(\vec{I};x_c,\tilde{F})}{\partial \tilde{F}}\right)$$

$$
\begin{aligned}
= \quad & \mathbb{E}_{I_1,\ldots,I_n}\left(\sum_i \sum_j \frac{I_i \cdot I_j}{\lambda_i(x_c,\tilde{F}) \cdot \lambda_j(x_c,\tilde{F})} \cdot g_j \cdot \frac{\partial \lambda_i(x_c,\tilde{F})}{\partial x_c} - \sum_i \sum_j \frac{I_i}{\lambda_i(x_c,\tilde{F})} \cdot g_j \cdot \frac{\partial \lambda_i(x_c,\tilde{F})}{\partial x_c}\right) \\
& -\mathbb{E}_{I_1,\ldots,I_n}\left(\sum_i \sum_j \frac{I_j}{\lambda_j(x_c,\tilde{F})} \cdot g_j \cdot \frac{\partial \lambda_i(x_c,\tilde{F})}{\partial x_c}\right) + \sum_i \sum_j g_j \cdot \frac{\partial \lambda_i(x_c,\tilde{F})}{\partial x_c} \\
= \quad & \mathbb{E}_{I_1,\ldots,I_n}\left(\sum_i \frac{I_i^2}{\lambda_i(x_c,\tilde{F})^2} \cdot g_i \cdot \frac{\partial \lambda_i(x_c,\tilde{F})}{\partial x_c}\right) + \mathbb{E}_{I_1,\ldots,I_n}\left(\sum_i \sum_{j \neq i} \frac{I_i \cdot I_j}{\lambda_i(x_c,\tilde{F}) \cdot \lambda_j(x_c,\tilde{F})} \cdot g_j \cdot \frac{\partial \lambda_i(x_c,\tilde{F})}{\partial x_c}\right) \\
& - \sum_i \sum_j g_j \cdot \frac{\partial \lambda_i(x_c,\tilde{F})}{\partial x_c} \\
= \quad & \sum_i \frac{\left(\lambda_i(x_c,\tilde{F}) + \lambda_i(x_c,\tilde{F})^2\right)}{\lambda_i(x_c,\tilde{F})^2} \cdot g_i \cdot \frac{\partial \lambda_i(x_c,\tilde{F})}{\partial x_c} + \sum_i \sum_{j \neq i} g_j \cdot \frac{\partial \lambda_i(x_c,\tilde{F})}{\partial x_c} - \sum_i \sum_j g_j \cdot \frac{\partial \lambda_i(x_c,\tilde{F})}{\partial x_c} \\
= \quad & \sum_i \frac{g_i}{\lambda_i(x_c,\tilde{F})} \cdot \frac{\partial \lambda_i(x_c,\tilde{F})}{\partial x_c} \qquad \text{(B5)}
\end{aligned}
$$

Under a Gaussian PSF, we can also verify using equations (5), (6), (8), and (13), and replacing them in equation (B5) that:

$$
\mathcal{I}_{1,2}(n) = \frac{1}{2\pi\sigma^2} \cdot \frac{F}{B} \cdot \sum_{i=1}^{n} \frac{\left(e^{-\gamma(x_i^- - x_c)} - e^{-\gamma(x_i^+ - x_c)}\right) \cdot J_i(x_c)}{\left(1 + \frac{1}{\sqrt{2\pi}\,\sigma} \cdot \frac{F}{B} \cdot J_i(x_c)\right)}. \qquad \text{(B6)}
$$

Of course, by symmetry, $\mathcal{I}_{1,2} = \mathcal{I}_{2,1}$.

Finally, for the last matrix element, one has:

$$
\begin{aligned}
\mathcal{I}_{2,2}(n) \equiv \quad & \mathbb{E}_{I_1,\ldots,I_n}\left(\left(\frac{\partial \ln L(\vec{I};x_c,\tilde{F})}{\partial \tilde{F}}\right)^2\right) \\
= \quad & \mathbb{E}_{I_1,\ldots,I_n}\left(\sum_i \sum_j \left(\frac{I_i \cdot I_j}{\lambda_i(x_c,\tilde{F}) \cdot \lambda_j(x_c,\tilde{F})} \cdot g_i \cdot g_j - 2 \cdot \frac{I_i}{\lambda_i(x_c,\tilde{F})} \cdot g_j\right)\right) + 1 \\
= \quad & \mathbb{E}_{I_1,\ldots,I_n}\left(\sum_i \left(\frac{I_i}{\lambda_i(x_c,\tilde{F})} \cdot g_i\right)^2\right) + \mathbb{E}_{I_1,\ldots,I_n}\left(\sum_i \sum_{j \neq i} \frac{I_i \cdot I_j}{\lambda_i(x_c,\tilde{F}) \cdot \lambda_j(x_c,\tilde{F})} \cdot g_i \cdot g_j\right) - 1 \\
= \quad & \sum_i \frac{\left(\lambda_i(x_c,\tilde{F}) + \lambda_i(x_c,\tilde{F})^2\right)}{\lambda_i(x_c,\tilde{F})^2} \cdot g_i^2 + \sum_i \sum_{j \neq i} g_i \cdot g_j - 1 \\
= \quad & \sum_i \frac{g_i^2}{\lambda_i(x_c,\tilde{F})}, \qquad \text{(B7)}
\end{aligned}
$$

where we have used the fact that $\sum_i g_i = 1$. In the case of a Gaussian PSF, it is easy to verify using equations (5), (6), (8), and (13) and replacing them in equation (B7) that:

$$
\mathcal{I}_{2,2} = \frac{1}{2\pi\sigma^2} \cdot \frac{1}{GB} \cdot \sum_{i=1}^{n} \frac{J_i(x_c)^2}{\left(1 + \frac{1}{\sqrt{2\pi}\,\sigma} \cdot \frac{F}{B} \cdot J_i(x_c)\right)}. \qquad \text{(B8)}
$$

To conclude, the inverse of the Fisher matrix, which is what we require to obtain the Cramér-Rao bound, would thus be given by:

$$
\mathcal{I}(n)^{-1} = \frac{1}{\Delta} \cdot \begin{pmatrix} \mathcal{I}_{22} & -\mathcal{I}_{12} \\ -\mathcal{I}_{12} & \mathcal{I}_{11} \end{pmatrix} \qquad \text{(B9)}
$$

where $\Delta = \mathcal{I}_{11} \cdot \mathcal{I}_{22} - \mathcal{I}_{11}^2$ is the determinant of the Fisher matrix.

Rene A. Mendez acknowledges partial support from project PFB-06 CATA-CONICYT and from project IC120009 "Millennium Institute of Astrophysics (MAS)" of the Iniciativa Cientfica Milenio del Ministerio de Economa, Fomento y Turismo de Chile. Jorge F. Silva and Rodrigo Lobos acknowledges support from FONDECYT - CONICYT grant # 1140840. We would also like to acknowledge several useful comments from an anonymous referee which lead to a better discussion of Section 3.3 and the introduction of Section 3.4 and Tables 1 and 2.

REFERENCES

Adorf, H.-M. 1996, Astronomical Data Analysis Software and Systems V, 101, 13

Baltay, C., Rabinowitz, D., Hadjiyska, E., et al. 2013, PASP, 125, 683

Cramér, H. 1946, Mathematical Methods of Statistics (Princeton: Princeton University Press)

Djorgovski, S. G., Drake, A. J., Mahabal, A. A., et al. 2011, arXiv:1102.5004

Gatewood, G., Stein, J., Difatta, C., Kiewiet de Jonge, J., & Breakiron, L. 1985, AJ, 90, 2397

Gillon, M., Jehin, E., Magain, P., et al. 2011, European Physical Journal Web of Conferences, 11, 6002

Jakobsen, P., Greenfield, P., & Jedrzejewski, R. 1992, A&A, 253, 329

King, I. R. 1983, PASP, 95, 163

Mendez, R. A., Costa, E., Pedreros, M. H., et al. 2010, PASP, 122, 853

Mendez, R. A., Silva, J. F, and Lobos, R. 2013, PASP, 125, 580.

Perryman, M. A. C., Jakobsen, P., Colina, L., et al. 1989, A&A, 215, 195

Pollacco, D. L., Skillen, I., Collier Cameron, A., et al. 2006, PASP, 118, 1407

Rao, C. R. 1945, Bull. Calcutta Math. Soc., 37, 81

Schroeder, D. J., 2013 in Astrometry for Astrophysics: Methods, models and Applications. (New York: Cambridge University Press): Geometrical Optics and Astrometry.

Selman, F. J. 2004, Proc. SPIE, 5493, 453

Stoica, P., and Moses, R.L. 1990, Signal Processing, 21, 349

Stuart, A., Ord, J. K., & Arnold S. 2004, Kendall's Advanced Theory of Statistics: Classical Inference and the Linear Model (Volume 2A) (New York: Oxford University Press)

Warner, B. D. 2006, A Practical Guide to Lightcurve Photometry and Analysis (New York: Springer)

Zaccheo, T. S., Gonsalves, R. A., Ebstein, S. M., & Nisenson, P. 1995, ApJ, 439, L43

Zhilyaev, B. E., Romanyuk, Y. O., Verlyuk, I. A., Svyatogorov, O. A., & Lovkaya, M. N. 2005, Kinematika i Fizika Nebesnykh Tel Supplement, 5, 528

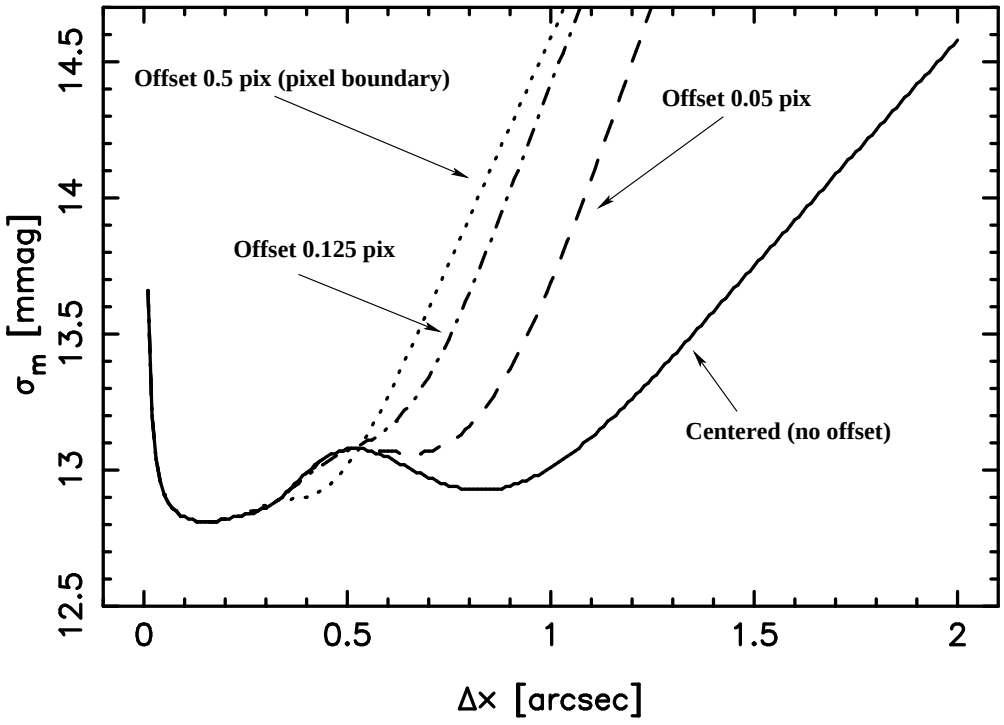

Fig. 1.— Photometric Cramér-Rao bound as given by the Fisher matrix coefficients in equation (18), in milli-magnitudes, as a function of detector pixel size Δx in arcsec. The curves were computed for a detector with $RON = 5$ e$^-$, $D = 0$ e$^-$, $G = 2$ e$^-$/ADU, a background of $f_s = 2\,000$ ADU/arcsec (representative of ground-based observations on moonless nights through optical broad-band filters with 600 sec exposure time on a good site), and for a Gaussian source with $FWHM = 0.5$ arcsec and $F = 5\,000$ ADU (corresponding to a $S/N \sim 80$). The solid, dashed, dot-dashed, and dotted lines are for sources which are centered, off-center by 0.05, 0.125 and 0.5 pix (equal to the pixel boundary) respectively. Compare with Figure 1 in Mendez et al. (2013).

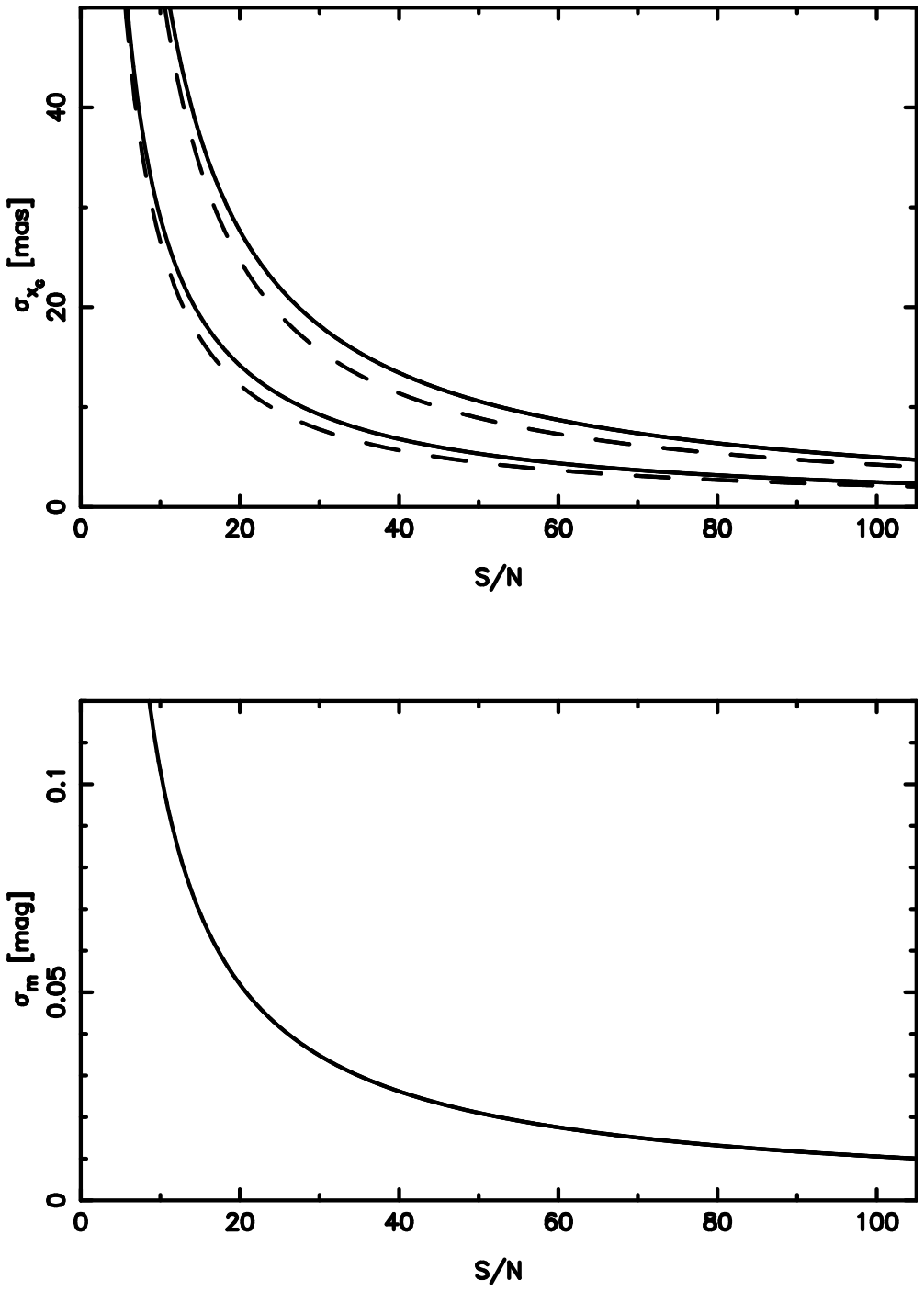

Fig. 2.— Astrometric (top) and photometric (bottom) Cramér-Rao limits as given by equation (18) as a function of S/N for a Gaussian source. All the curves were computed for the same detector parameters as those of Figures 1, with $\Delta x = 0.2$ arcsec and the source centered on a pixel. In the upper figure, the solid lines correspond to a $FWHM = 1.0$ arcsec (upper line) and $FWHM = 0.5$ arcsec (lower line), both with $f_s = 2\,000$ ADU/arcsec. The corresponding dashed lines are the predictions for the same two $FWHM$, but with no background ($f_s = 0$ ADU/arcsec), the only source of noise comes in this case from the readout electronics. In the lower panel, the curves for $FWHM = 1.0$ and 0.5 arcsec, as well as for $f_s = 2\,000$ and 0 ADU/arcsec overlap with each other - see text for a discussion.

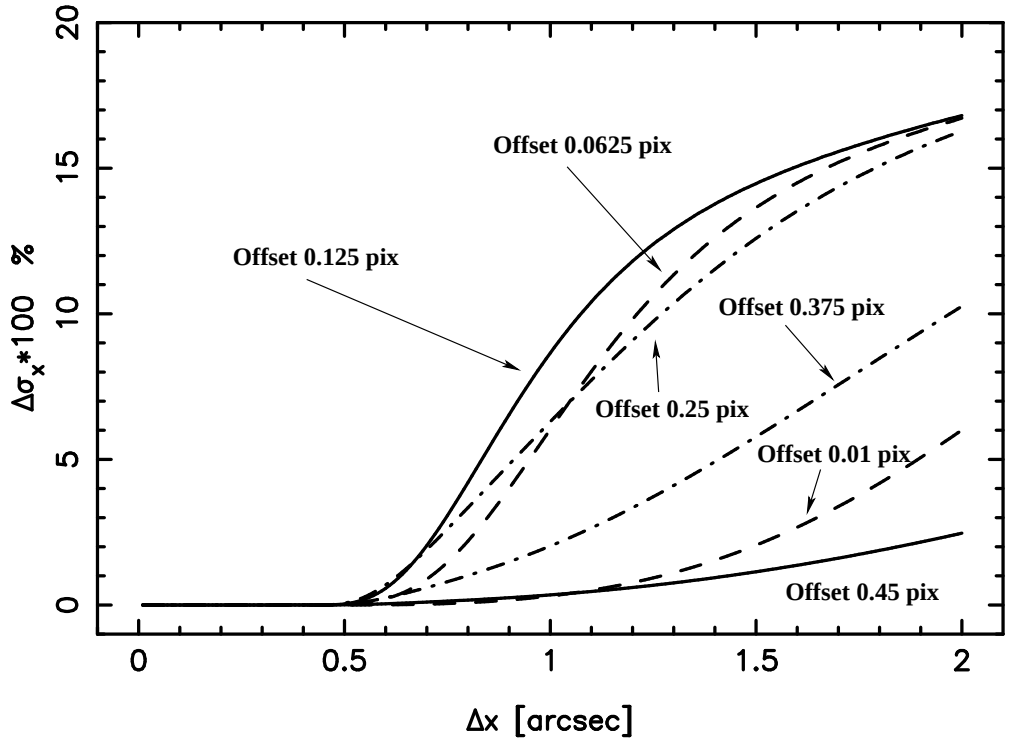

Fig. 3.— Fractional difference in the Cramér-Rao bound computed in 2D and 1D, as a function of detector pixel size for the same detector parameters as those of Figures 1, and for a source with $FWHM = 0.5$ arcsec, $F = 5\,000$ ADU, and $f_s = 2\,000$ ADU/arcsec ($S/N \sim 80$). The upper (lower) solid line is for a pixel offset of 0.125 pix (0.45 pix), the upper (lower) dashed line is for a pixel offset of 0.0625 pix (0.01 pix), and the upper (lower) dot-dashed lines is for a pixel offset of 0.25 pix (0.375 pix) respectively. Note: The pairing of line types is done only to avoid crowding of the figure.

Table 1. Effect of under-sampling, pixel offset, and S/N on the Cramér-Rao limit.

		$S/N = 5$		$S/N = 30$		$S/N = 100$	
Δx arcsec	Offset pix	σ_{x_c}, $\sigma_{x_{c_{1D}}}$ mas	$\sigma_{\tilde{F}}$, $\sigma_{\tilde{F}_{1D}}$ %	σ_{x_c}, $\sigma_{x_{c_{1D}}}$ mas	$\sigma_{\tilde{F}}$, $\sigma_{\tilde{F}_{1D}}$ %	σ_{x_c}, $\sigma_{x_{c_{1D}}}$ mas	$\sigma_{\tilde{F}}$, $\sigma_{\tilde{F}_{1D}}$ %
0.25	0.125	54 , 54	18, 18	8.7, 8.7	3, 3	2.5, 2.5	1, 1
0.5	0.125	87 , 85	18, 18	13, 13	3, 3	3.2, 3.2	1, 1
1.0	0.125	443, 341	26, 20	60, 50	4, 3.5	12, 11	1, 1
1.5	0.125	3930, 2831	32, 23	529, 408	4.6, 3.6	102, 89	1, 1
0.25	0.25	54 , 54	18, 18	8.7, 8.7	3, 3	2.5, 2.5	1, 1
0.5	0.25	69 , 67	19, 18	11, 11	3, 3	3.0, 3.0	1, 1
1.0	0.25	173, 140	26, 21	24, 21	4, 3.5	5.3, 5.1	1, 1
1.5	0.25	541, 403	32, 24	73, 58	4, 3	15, 13	1, 1

Note. — All Cramér-Rao estimates used a detector with $G = 2$ e$^-$/ADU, $RON = 5$ e$^-$ and no dark noise, a background of $f_s = 2\,000$ ADU/arcsec, and a source with a $FWHM = 0.5$ arcsec (same values as for Figure 3). The upper part of the table is for a pixel offset of 0.125 pix, while the lower part is for a pixel offset of 0.25 pix, see text for details.

Table 2. Effect of changes in the $FWHM$ and the background on the Cramér-Rao limit of under-sampled images.

		$S/N = 5$		$S/N = 30$		$S/N = 100$	
$FWHM$	f_s	σ_{x_c}	$\sigma_{\tilde{F}}$	σ_{x_c}	$\sigma_{\tilde{F}}$	σ_{x_c}	$\sigma_{\tilde{F}}$
arcsec	ADU arcsec^{-1}	mas	%	mas	%	mas	%
0.5	2000	1092	19	147	3	29	1
0.6	2000	562	20	76	3	15	1
0.5	2200	1145	20	155	3	30	1
0.6	2200	589	21	80	3	16	1
0.5	2000	70	26	11	4	3	1
0.6	2000	84	26	13	4	4	1
0.5	2200	73	27	11	4	3	1
0.6	2200	88	27	13	4	4	1

Note. — All Cramér-Rao estimates used a detector with $G = 2$ e$^-$/ADU, $RON = 5$ e$^-$ no dark noise, and $\Delta x = 1.0$ arcsec, a background of $f_s = 2\,000$ ADU/arcsec, and a source with a $FWHM = 0.5$ arcsec (same values as for Figure 3). The upper part of the table is for a source with no offset (i.e., centered on a pixel, worst case for astrometry, best case for photometry), whereas the lower part is for a source at a pixel boundary (best case for astrometry, worst case for photometry).